DOE/NV/03624--0660

Shock Hugoniot of forged and additively manufactured 304L stainless steel

Sarah A. Thomas[1,a)], M. Cameron Hawkins[2], Robert S. Hixson[1], George T. Gray III[3], and Saryu J. Fensin[3]

[1]Nevada National Security Site, New Mexico Operations, Los Alamos, New Mexico 87544, USA
[2]Nevada National Security Site, Nevada Operations, Las Vegas, Nevada 89030, USA
[3]Los Alamos National Laboratory, MST-8 Group, Los Alamos, New Mexico 87545, USA

[a)]Electronic mail: ThomasSA@nv.doe.gov

The purpose of this research was to measure the equation of state for additively manufactured (AM) and forged 304L stainless steel. An understanding of the dynamic behavior of AM metals is integral to their timely adoption into industrial and governmental applications. The Hugoniot of the AM 304L was compared to that of the forged 304L. This comparison enabled us to determine the sensitivity of the equation of state to processing parameters and the resulting microstructure. Our results show that there is a measurable difference in the Hugoniot between the AM 304L and forged 304L. The shock wave velocities for the AM 304L were found to be slower than those for the forged 304L at similar particle speeds perhaps because of the presence of porosity in the AM 304L. While our measurements of density showed no distinct trend toward a measurable decrease in density in the AM 304L, there was a fair amount of scatter in these results.

I. INTRODUCTION

Additively manufactured (AM) materials are becoming more prevalent in many real-world applications because they offer some advantages over materials manufactured via standard manufacturing processes. For example, parts can be printed to near net shape with minimal machining and in a relatively short time, which aids in the fast and efficient production of prototypes. It is also relatively easy to make changes to part designs on the fly. The potential value of using AM materials in various applications in both the government and commercial sectors drives the need for better understanding of their dynamic behavior. Moving forward requires a path toward certification of required properties.

Research in this area has made significant strides in recent years, primarily in measuring properties like quasi-static and dynamic strength of AM materials. Many groups have performed quasi-static tensile and

yield strength measurements along with a thorough characterization of the microstructure.[1–5] A group that performed tensile tests on AM stainless steel found that void distributions had a large effect on fracture mechanisms; inhomogeneous void distributions resulted in flaws developing at the voids, whereas randomly distributed voids led to fractures more typical of wrought metal.[1] A study of tensile damage evolution in AM stainless steel noted that the coalescence of voids was the main mechanism of damage for AM parts, an effect that was more pronounced at higher levels of initial porosity.[2] A team that investigated the influence of the manufacturing process of grade 316L stainless steel on the microstructure and resulting material properties found that mechanical properties like tensile and yield strength depend strongly on both manufacturing process and orientation.[3] The results of this investigation were similar to those of an earlier study done on Ti-6Al-4V by a different group.[4] Another experimental study in which AM 316L steel parts were subjected to fatigue reported a decrease in the number of dislocations and an increase in twinning.[5]

Other groups have focused on dynamic strength properties like spall.[6–8] A study on the spall strength of AM Ti-6Al-4V samples showed much greater spall strength when loading was applied parallel versus normal to the AM build layer interfaces.[6] Another group that studied Ti-6Al-4V samples examined the effects of voids on dynamic strength, finding that denser samples displayed greater strength, while ductility remained comparable whether the samples were dense or porous.[7] A study done on 316L stainless steel found that the AM material had a higher yield strength than the wrought material and that while the wrought material had a spall strength that remained invariant to peak shock stress, the spall strength of the AM material diminished with increased shock loading.[8]

Few studies, however, have examined the equation-of-state properties of AM materials, even though equation-of-state properties are important in understanding the overall dynamic behavior of AM materials when used in extreme environments or applications. One study that compared the equation of state of AM 304L stainless steel with that of conventionally wrought 304L stainless steel found no difference between the two.[9] However, more research in this area is needed. In this study, we focused on measuring the shock

Hugoniot of AM 304L stainless steel. A knowledge of dynamic strength properties, shock Hugoniot, and dislocation dynamics of materials are critical to predicting their behavior during dynamic events.

II. EXPERIMENTAL METHODS

To make dynamic measurements of the relevant properties of AM 304L stainless steel, we used conventional shock compression techniques along with a top-hat method to accurately determine the shock velocity. Because this metal was manufactured with a directional printing technique, we wished to investigate the directional dependence of dynamic properties. To achieve this goal, we obtained samples from a manufactured plate in the directions we wished to use for our experiments. In this section we describe the manufacturing process in more detail and elaborate on how we conducted our experiments to make careful measurements of shock and particle velocity.

A. Material and additive manufacturing processing

Metallic samples can be manufactured by various AM techniques. For example, one can utilize lasers to melt wire samples and build up bulk samples by laying down weldments. This process is very similar to metal inert gas (MIG) welding methods. One can also use a powder bed method to laser fuse metallic powders with a rastering technique; this is the method we used to manufacture samples for this study. For this method to work well, it is necessary to start with pure powder with little surface oxide. We must also optimize this method to produce samples that are close to full density and have very little to no internal porosity. We can determine the purity of samples made this way via metallurgical methods. We can also determine the presence of significant porosity by measuring shock velocity. By significant porosity we mean that the pore compaction process is significant enough to alter the Hugoniot of the material. It is known from past research that even relatively little porosity will lower the measured shock velocity and cause shock temperatures to increase rapidly.[10,11] Of note is that even a 1% drop in porosity from full density can result in as much as a 3% difference in shock Hugoniot values.

Any AM process produces artifacts in the sample that influence crystallographic and grain morphology. For example, there can be an orientation of grains along and normal to the direction of rastering when the powder is fused. In some cases, columnar grains can also be produced. In this way, AM grain structures differ from those observed in samples produced by conventional casting and/or forging methods, which tend to be equiaxed and have a random texture. Anisotropy seems to be more pronounced in AM metals and can result in highly directional response for some properties. The effect of this anisotropy on shock properties is still under study.

A single lot of pedigreed micro-melt 304L stainless steel powder (termed ADET powder) manufactured by Carpenter Powder Products in Sweden was used for manufacturing the AM material. A detailed chemistry analysis of this powder is shown in Table I.

TABLE I. The measured chemical composition of the 304L stainless steel powder (ADET).

Element	wt %	Element	wt%
C	0.015	Mo	0.0
Si	0.53	Ti	0.0
Mn	1.5	Nb	0.0
P	0.012	Cu	0.0
S	0.003	N	0.05
Cr	18.4	O	0.019
Ni	9.8	Fe	Balance

The powder has a chromium-to-nickel equivalent ratio of 1.70, apparent density of 4.20 g/cm^3, and tap density of 4.80 g/cm^3. The plates fabricated on the EOS GmbH Electro Optical Systems M 280 system were built on a 50.5 mm thick AISI 304L baseplate in the vertical and horizontal directions as shown in Fig. 1. The processing parameters used were the EOS-developed PH1 20 μm settings. This license from EOS was developed specifically for stainless steel and uses rotational rectilinear hatching with 20 μm layer heights. However, due to the proprietary nature of the fabrication method, the only detail that was known during the fabrication was the layer height.

FIG. 1. Optical photograph of EOS builds on 304L stainless steel baseplate.

The plate from which we obtained our samples was manufactured by the Sigma Division at Los Alamos National Laboratory (LANL), with raster directions set at 0, 90, and 45 degrees. Figure 2 depicts this plate and shows the locations from which we obtained the samples. These included two large samples in the *z*-direction and many smaller samples at various orientations. The specific samples we studied are Z1a, X1, XY1(+45), and XY2(+45).

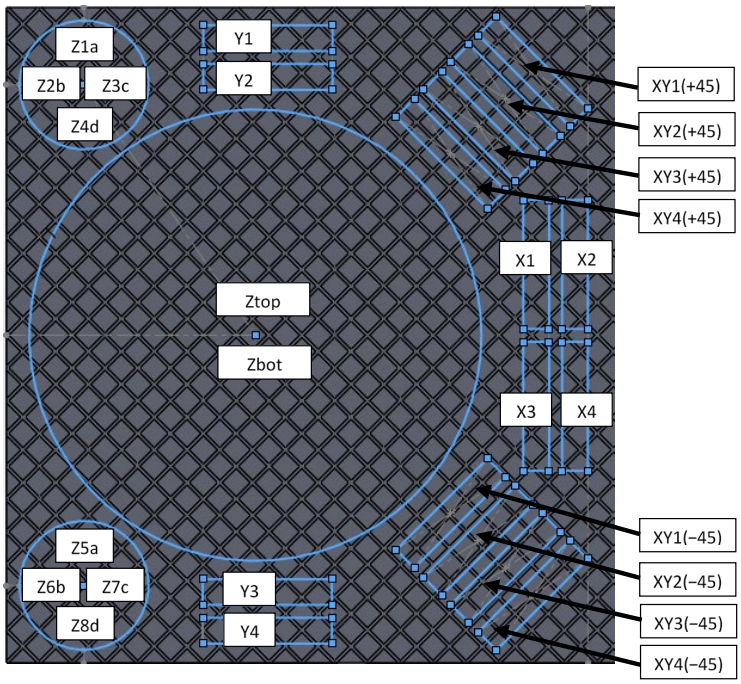

FIG. 2. LANL AM 304L plate and locations from which samples were taken for dynamic experiments.

Figure 3 contrasts the microstructure produced on the EOS powder-bed AM machine using the pedigreed 304L stainless steel powder with the microstructure of the forged 304L stainless steel. The overall microstructure of the EOS build material is observed to be significantly finer macroscopically than that of the forged material. An equiaxed polycrystalline microstructure typical of many recrystallized metals and alloys is evident in the forged 304L stainless steel. No ferrite phase was observed in the EOS build plate.

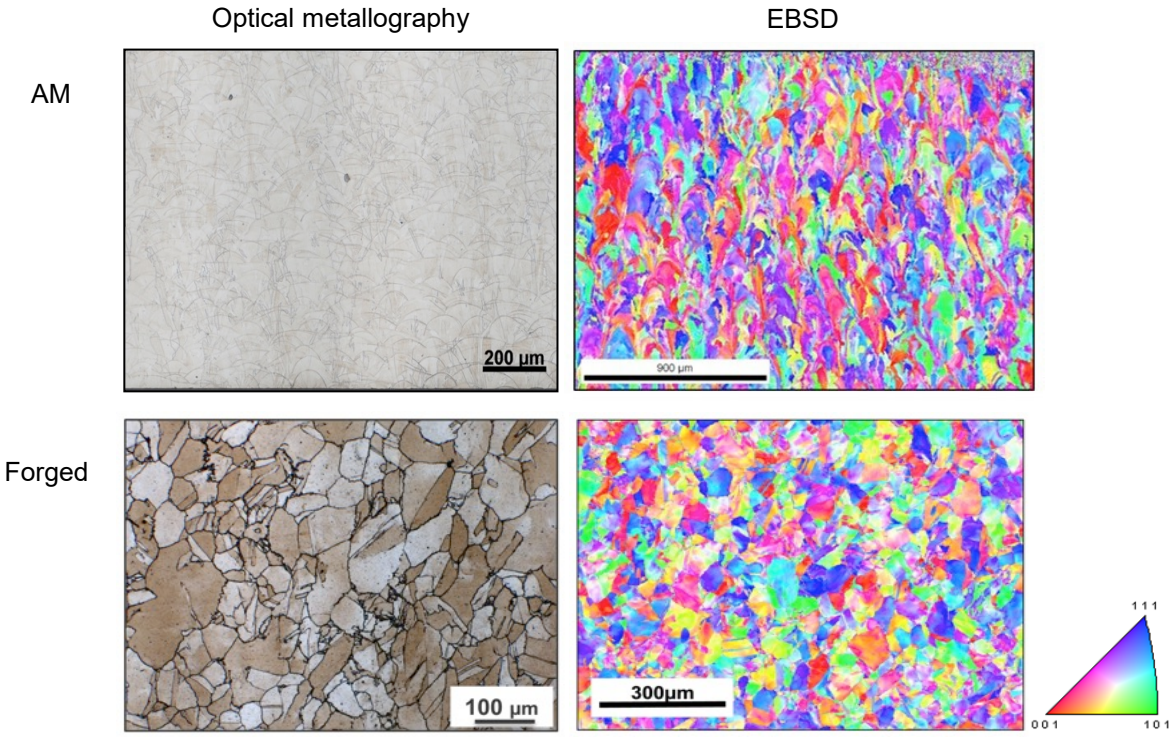

FIG. 3. Optical metallography and electron backscatter diffraction (EBSD) scans of AM 304L stainless steel microstructure and forged 304L stainless steel microstructure.

B. Hugoniot measurements

All samples were metrologized prior to impact experiments. As part of this process, we determined the ambient longitudinal and shear sound speeds using the pulse-echo technique and performed immersion density measurements. Sound speeds are estimated to be accurate to about 0.5%, while immersion densities are estimated to be good to approximately 1%. Thicknesses were measured after the samples were lapped flat and parallel to within 5 to10 µm. These values are shown in Table II.

TABLE I. Measured thicknesses, densities, and longitudinal and shear sound speeds of the samples.

Experiment number	Material	Thickness (mm)	Density (g/cm^3)	Sound speed (km/s)	
				Longitudinal	Shear
172	Forged	2.010 ±0.010	7.86 ±0.08	5.78 ±0.08	3.15 ±0.06
173	AM-XY1	1.997 ±0.010	7.87 ±0.08	5.77 ±0.08	3.10 ±0.06
174	AM-Z1a	1.999 ±0.010	7.87 ±0.08	5.72 ±0.08	3.20 ±0.06
176	AM-XY2	2.001 ±0.010	7.90 ±0.08	5.80 ±0.08	3.12 ±0.06
177	AM-X1	1.996 ±0.010	7.83 ±0.08	5.80 ±0.08	3.16 ±0.06

We conducted quartz top-hat experiments to measure the forged material as well as the *z*-, *xy*-, and *x*-directions of the AM material. For these experiments, the impactor was a quartz disc backed by syntactic foam. The target was a quartz baseplate with the same dimensions (35 mm diameter by 2 mm thick) as the impactor. The sample material (304L), with the same thickness (2 mm) and a smaller diameter (10 mm), was bonded to the quartz baseplate by thin glue bond methods. Finally, we glued a sapphire window (10 mm diameter by 12 mm thick) to the back of the target to reduce elastic-plastic wave interactions due to reflectance from the free surface. A sketch of this experimental design is shown in Fig. 4.

The projectiles were launched at a nominal velocity of 400 m/s. Four 2-fiber photonic Doppler velocimetry (PDV) probes[12] were placed at opposite sides around the brim of the quartz baseplate. These four probes not only act as accurate timing fiducials for the arrival of the shock wave at the back surface of the 304L sample, but also provide cross-timing information. Because quartz remains elastic in the stress regime of this study, only a single wave propagates into the sample. (It is important to note that this technique is limited to stress states below which quartz stays elastic; for *z*-cut quartz, this is ~8.5 GPa.) Two additional 2-fiber probes illuminated the center of the sample through the sapphire window to provide information regarding the timing of the elastic and plastic waves exiting the sample. The difference between the entrance and exit times of the shock wave proves the transit time for the shock to travel though the sample. This information, coupled with the thickness of the samples, provides measurements for the shock wave velocity with an accuracy of about 1%.

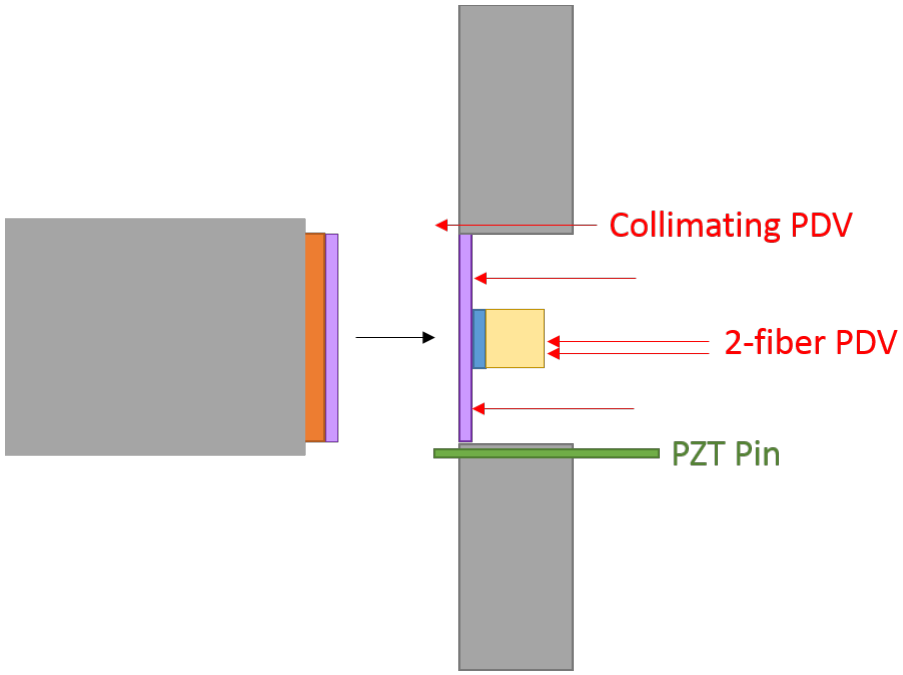

FIG. 1. Quartz top-hat experimental design. The projectile and target plates are shown in gray. Affixed to the front of the projectile is the syntactic foam backing (orange) and the quartz impactor (purple). The target is centered on the target plate and is comprised of a quartz baseplate (purple), the 304L sample (blue), and a sapphire window (yellow). A single collimating probe measures the projectile velocity. There are two 2-fiber probes in the center, one slightly offset from the center of the target, and four additional 2-fiber probes that circle the quartz baseplate at a fixed radius (11.25 mm). The design also includes a single piezoelectric (PZT) pin (green) that serves as a diagnostics trigger.

III. RESULTS

We used the quartz top-hat method to measure the Hugoniot of both the forged and AM 304L stainless steel samples. Due to anisotropy in the microstructure of the AM 304L stainless steel, measurements were performed along the various directions. These experiment results are shown in Table III.

TABLE III. Impactor velocity (U_D), particle velocity (u_p), and shock velocity (U_S) measurements from the quartz top-hat experiments.

Experiment number	Material	Velocity (km/s)		
		Impactor, U_D	Particle, u_p	Shock, U_s
172	Forged	0.399 ±0.003	0.128 ±0.002	4.77 ±0.05
173	AM-XY1	0.400 ±0.003	0.131 ±0.002	4.68 ±0.05
174	AM-Z1a	0.400 ±0.003	0.132 ±0.002	4.64 ±0.05
176	AM-XY2	0.400 ±0.003	0.132 ±0.002	4.66 ±0.05
177	AM-X1	0.395 ±0.003	0.130 ±0.002	4.59 ±0.05

Figure 5 shows plots of experiments 172 (forged 304L) and 177 (AM 304L, X1). The velocimetry curves are plotted such that the elastic waves are aligned in time. The plastic wave arrives earlier for the forged sample because of the higher shock velocity, U_s.

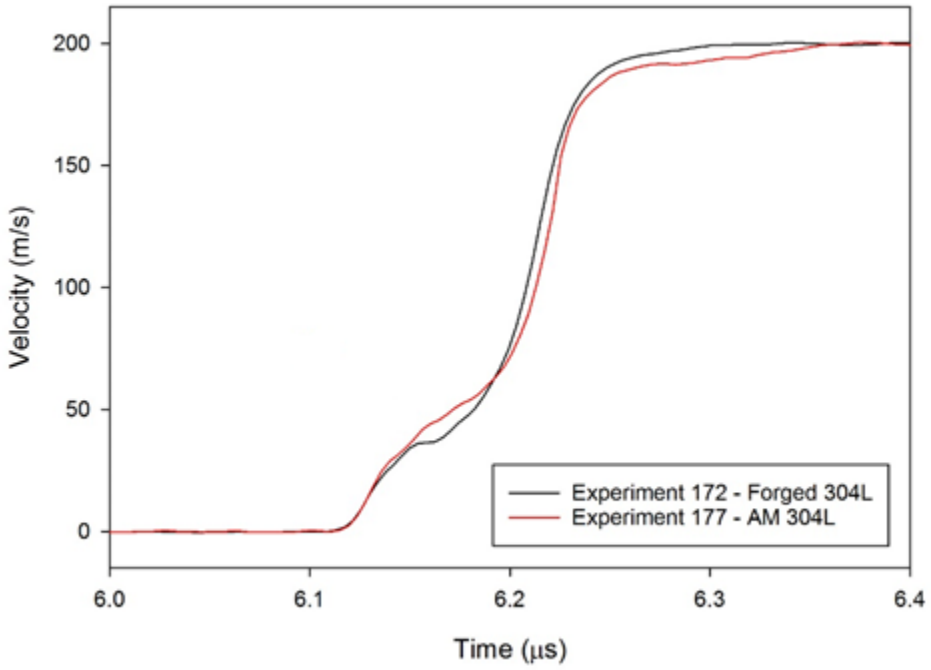

FIG. 2. Overplot of velocimetry data from experiments 172 (forged 304L) and 177 (AM 304L, X1) with aligned elastic waves.

Figure 6 shows an example of the wave profile in the quartz baseplate. We determine the time the shock enters the sample from this wave. The front of the profile, where it sharply rises above the background, marks where the impact between the quartz impactor and baseplate occurs. The signal then plateaus, which indicates that at this point, the wave is traveling through the baseplate. The sharp drop at the end is the time at which the wave exits the baseplate and enters the sample; for our calculations, we designate this point in time as the timing fiducial.

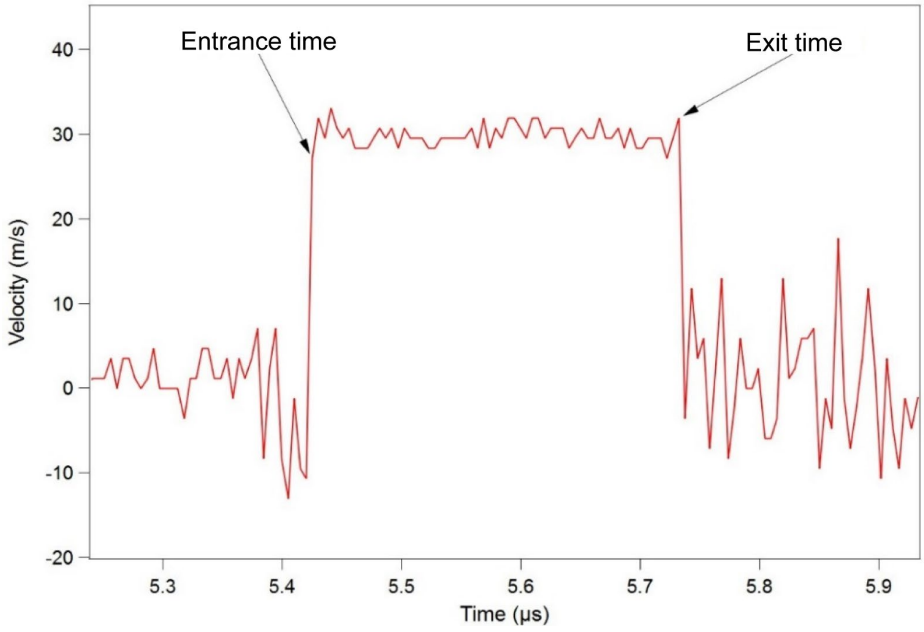

FIG. 3. Velocity profile in the quartz baseplate. The sharp rise occurs when the shock enters the quartz baseplate, and the drop in the velocity indicates when the shock leaves the baseplate and enters the target sample.

By averaging the exit times from the four probes, we can determine when the wave exits the center of the quartz with an accuracy of 1 to 2 ns. Another way of determining an accurate exit time is to plot the exit times from each of the four probes versus the angle at which the probe sits with respect to the center of the target, then fit those points to a sine wave. The equation for the sine wave is

$$y = y_0 + A\sin(fx + \varphi)\,, \tag{1}$$

where A is the amplitude of the wave, f is the frequency, and φ is the phase. The constant, y_0, is the midline of the sine curve and the time at which the shock enters the front of the target. An example fit is shown in Fig. 7.

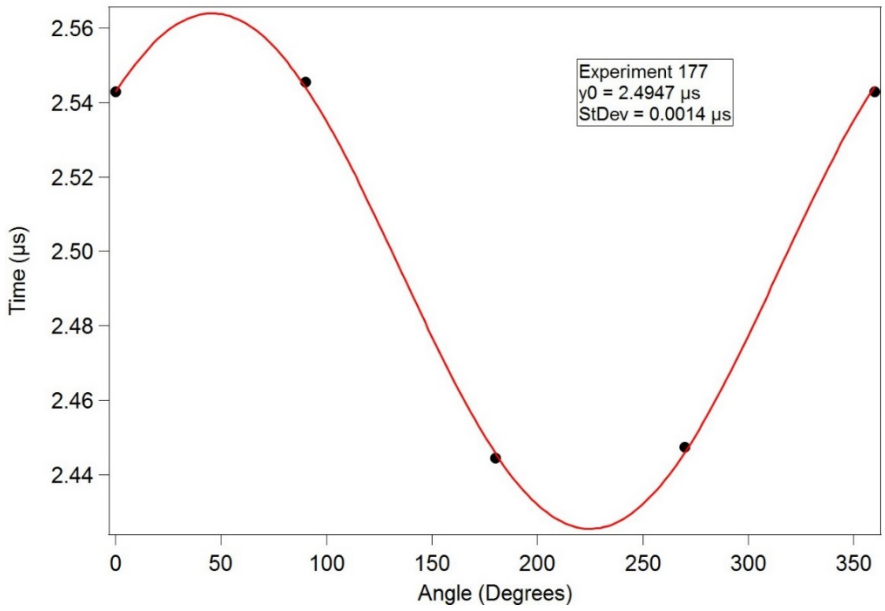

FIG. 4. Sine fit of the exit times taken from the outer probes for experiment 177.

The particle and shock velocity results presented in Table III are plotted over the extrapolated shock Hugoniot for 304L stainless steel from work done at Los Alamos Scientific Laboratory (LASL)[13] and shown in Fig. 8. This work, *LASL Shock Hugoniot Data*, is a compendium of Hugoniot data released by LASL (LANL's predecessor) in 1980. We calculated the shock velocities using the average of the exit times from the quartz baseplate collected by the four PDV probes and subtracting that time from the plastic wave arrivals at the back of the target, then dividing it into the thickness of the target, as shown by

$$U_S = \frac{x_{\text{target}}}{t_{\text{steel}} - t_{\text{quartz}}}, \tag{2}$$

where U_S is the shock velocity, x_{target} is the thickness of the target, and t_{steel} and t_{quartz} are the times the plastic wave exits the steel target and quartz baseplate, respectively.

Particle velocities were calculated from the measured impactor velocity and shock speed in the target. We calculated the particle velocity using the measured shock speed in the target and the known Hugoniot for quartz to impedance match between the quartz and the steel target. Uncertainties associated with the calculations are estimated to be between 1.0% and 1.5%.

Figure 8 shows that there is a notable difference between the AM 304L shock velocities and the data derived from the LASL Hugoniot data.[13] The LASL data, however, match our forged 304L results quite well, lying well within our estimated limits of error. All of the AM Hugoniot points are lower than the forged metal Hugoniot points to some degree. We estimated error in shock velocities by using the sum of the squares of the error in determining the travel time of the plastic wave and in measuring the thickness of the samples, such that

$$\frac{\Delta U_s}{U_s} = \sqrt{\left(\frac{\Delta t}{t}\right)^2 + \left(\frac{\Delta x}{x}\right)^2}, \tag{3}$$

where U_s is the shock velocity, t is the time, x is the sample thickness, and ΔU_s, Δt, and Δx are the errors in those values. We estimated the error in determining the travel time to be from 3 to 4 ns out of ~440 ns and the error in measuring the thickness of the sample to be around 10 μm out of 2000 μm (2 mm). This gives us an overall error of less than 1%, with the major contribution to the error coming from determining wave transit times. The relatively long rise time for the plastic (shock) wave because of the relatively low shock stress, in addition to the uncertainty involved in choosing the time of arrival for the midpoint of that rise, contributes significantly to timing uncertainty. The difference between our forged 304L result and the value derived from the LASL data for roughly the same particle velocity is around 0.5%, which is within our error bar. The differences between the AM results and the values from the LASL data range between 1.7% and 3.6%, falling well outside the estimated errors.

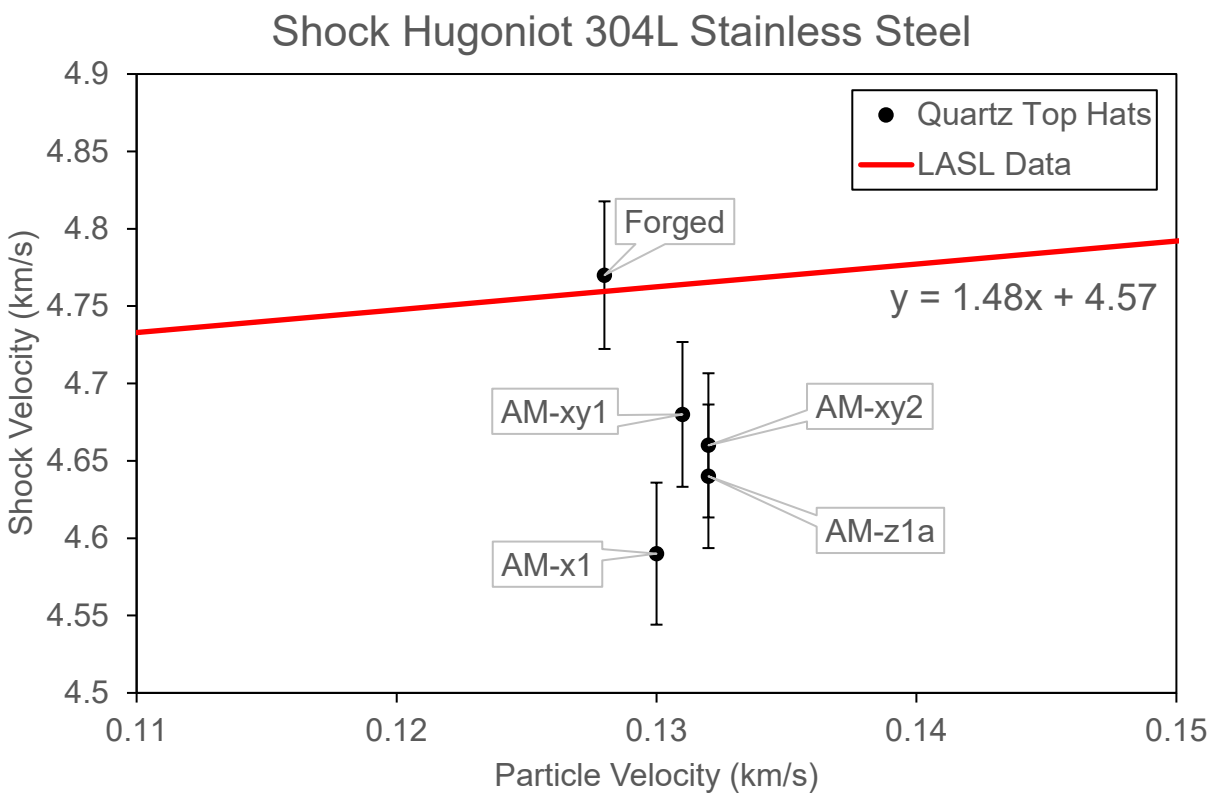

FIG. 5. Results from quartz top-hat experiments with 1% error bars plotted over the extrapolated shock Hugoniot for 304L stainless steel from the *LASL Shock Hugoniot Data*.[13]

We hypothesize that these results imply that there is some porosity in the AM material, although we could not measure it using immersion density. There were relatively large errors (on the order of 1%) in our density measurements. However, it has been demonstrated by earlier research that even a 1% drop in density can lead to a drop in shock velocity of more than 2%.[10] This is close to the differences we see between the AM and forged material shock velocities. It is worth noting that other morphological factors could contribute to these observed shock velocity differences. However, porosity is the most likely cause.

IV. DISCUSSION AND CONCLUSIONS

Today AM processes are increasingly used for manufacturing metallic components for a broad range of applications. Some of these applications involve dynamic loading of the components. This drives a need to find out whether key dynamic properties of AM parts are similar enough to those of their forged

counterparts such that functionality will not be compromised. Much of the dynamic property characterization of AM metals has been limited to measuring dynamic compressive or tensile strength, while there is also a need to understand Hugoniot properties. In this work we have made careful measurements of shock Hugoniot properties for both forged and AM 304L stainless steel. Values for shock velocity, U_s, at a given particle velocity, u_p, are lower in the AM 304L than in the forged 304L by a measurable amount, as shown in Fig. 8. This difference is outside our estimated uncertainties for this type of experiment. The lower shock velocity in the AM material is almost certainly due to the lower porosity in the AM material. While the immersion densities of the forged and AM materials are very similar, there is a lot of scatter in these measurements. Because of this, we do not see a measurable trend in initial density that shows systematically lower densities for AM samples. Even a small amount of porosity can have a measurable effect on the shock velocities, as demonstrated in this work and reported by others. For example, earlier work done on iron at LASL showed that an 11% drop in density resulted in a 33% drop in shock velocities at particle velocities of around 0.6 km/s.[10] This difference lessens for higher particle velocities. However, for the particle velocities in our research (<0.15 km/s), a 1% drop in density could easily lead to a decrease of 2% or more in shock velocity.

Through a variety of different experiments, we were able to measure the shock Hugoniot of both forged and AM 304L stainless steel at a single shock stress and particle velocity state. While our measured Hugoniot point for the forged steel matched well (within 0.5%) with archival data from the *LASL Shock Hugoniot Data*,[13] the values for the AM steel were lower by a measurable amount (1.7% to 3.6%). This difference is likely due to a small amount of porosity in the AM samples. That even a small amount of porosity can have a marked effect on the shock velocities of a material may affect the use of AM materials in extreme conditions or applications. It seems unlikely that metals may be formed by this method without some porosity, which will mean slower shock velocities in these materials than in their forged counterparts.

ACKNOWLEDGMENTS

We gratefully acknowledge the support of the NNSS C3 Launcher team, including Jeff Cates, Russ Howe, James Majdanac, Melissa Matthes, and Todd Ware. This manuscript has been authored by Mission Support and Test Services, LLC, under Contract No. DE-NA0003624 with the U.S. Department of Energy, National Nuclear Security Administration, Office of Defense Programs (NA-10). The United States Government retains and the publisher, by accepting the article for publication, acknowledges that the United States Government retains a non-exclusive, paid-up, irrevocable, worldwide license to publish or reproduce the published form of this manuscript, or allow others to do so, for United States Government purposes. The U.S. Department of Energy will provide public access to these results of federally sponsored research in accordance with the DOE Public Access Plan (http://energy.gov/downloads/doe-public-access-plan). The views expressed in the article do not necessarily represent the views of the U.S. Department of Energy or the United States Government. DOE/NV/03624--0660.

REFERENCES

[1]H. D. Carlton, A. Haboub, G. F. Gallegos, D. Y. Parkinson, and A. A. MacDowell, "Damage evolution and failure mechanisms in additively manufactured stainless steel," *Mater. Sci. Eng. A* **651**, 406 (2016), https://doi.org/10.1016/j.msea.2015.10.073.

[2]A. Yadollahi, N. Shamsaei, Y. Hammi, and M. F. Horstemeyer, "Quantification of tensile damage evolution in additive manufactured austenitic stainless steels," *Mater. Sci. Eng. A* **657**, 399 (2016), https://doi.org/10.1016/j.msea.2016.01.067.

[3]A. Röttger, K. Geenen, M. Windmann, F. Binner, and W. Theisen, "Comparison of microstructure and mechanical properties of 316 L austenitic steel processed by selective laser melting with hot-isostatic pressed and cast material," *Mater. Sci. Eng. A* **678**, 365 (2016), https://doi.org/10.1016/j.msea.2016.10.012.

[4]M. Simonelli, Y. Y. Tse, and C. Tuck, "Effect of the build orientation on the mechanical properties and fracture modes of SLM Ti-6Al-4V," *Mater. Sci. Eng. A* **616**, 1 (2014), https://doi.org/10.1016/j.msea.2014.07.086.

[5]M. L. Pace, A. Guarnaccio, P. Dolce, D. Mollica, G. P. Parisi, A. Lettino, L. Medici, V. Summa, R. Ciancio, and A. Santagata, "3D additive manufactured 316L components microstructural features and changes induced by working life cycles," *Appl. Surf. Sci.* **418**, 437 (2017), https://doi.org/10.1016/j.apsusc.2017.01.308.

[6]D. R. Jones, S. J. Fensin, O. Dippo, R. A. Beal, V. Livescu, D. T. Martinez, C. P. Trujillo, J. N. Florando, M. Kumar, and G. T. Gray III, "Spall fracture in additive manufactured Ti-6Al-4V," *J. Appl. Phys.* **120**, 135902 (2016), https://doi.org/10.1063/1.4963279.

[7]R. Fadida, D. Rittel, and A. Shirizly, "Dynamic mechanical behavior of additively manufactured Ti6Al4V with controlled voids," *J. Appl. Mech.* **82**, 041004 (2015), https://doi.org/10.1115/1.4029745.

[8]G. T. Gray III, V. Livescu, P. A. Rigg, C. P. Trujillo, C. M. Cady, S. R. Chen, J. S. Carpenter, T. J. Lienert, and S. J. Fensin, "Structure/property (constitutive and spallation response) of additively manufactured 316L stainless steel," *Acta Mater.* **138**, 140 (2017), https://doi.org/10.1016/j.actamat.2017.07.045.

[9]J. L. Wise, D. P. Adams, E. E. Nishida, B. Song, M. C. Maguire, J. Carroll, B. Reedlunn, J. E. Bishop, T. A. Palmer, "Comparative shock response of additively manufactured versus conventionally wrought 304L stainless steel," *AIP Conf. Proc.* **1793**, 100015 (2017),https://doi.org/10.1063/1.4971640.

[10]R. G. McQueen, S. P. Marsh, J. W. Taylor, J. N. Fritz, and W. J. Carter, "The equation of state of solids from shock wave studies," in *High-Velocity Impact Phenomena*, ed. R. Kinslow (New York: Academic Press, 1970), 293–417, https://doi.org/10.1016/B978-0-12-408950-1.50012-4.

[11]R. F. Trunin, *Shock Compression of Condensed Materials* (Cambridge: Cambridge University Press, 1998), https://doi.org/10.1017/CBO9780511599835.

[12]O. T. Strand, D. R. Goosman, C. Martinez, T. L. Whitworth, and W. W. Kuhlow, "Compact system for high-speed velocimetry using heterodyne techniques," *Rev. Sci. Instrum.* **77**, 083108 (2006), https://doi.org/10.1063/1.2336749.

[13]S. P. Marsh, ed., *LASL Shock Hugoniot Data* (Berkeley: University of California Press, 1980), 214, http://large.stanford.edu/publications/coal/references/docs/shd.pdf.